

**Impacts of Assimilating Measurements of Different State Variables with a Simulated  
Supercell Storm and Three Dimensional Variational Method**

Guoqing Ge<sup>1</sup>, Jidong Gao<sup>2</sup>, and Ming Xue<sup>1,3</sup>

<sup>1</sup>*Center for Analysis and Prediction of Storms,  
University of Oklahoma, Norman, OK 73072*

<sup>2</sup>*National Severe Storm Laboratory, Norman, OK 73072,*

<sup>3</sup>*School of Meteorology, University of Oklahoma, Norman, OK 73072*

To be submitted to Journal of Applied Meteorology and Climatology

June 2012

Revised November 5, 2012

---

*Corresponding author address:* Dr. Guoqing Ge, Center for Analysis and Prediction of Storms,  
Suite 2500, 120 David L. Boren Blvd, Norman OK 73072

E-mail: [geguoqing@ou.edu](mailto:geguoqing@ou.edu)

## Abstract

This paper investigates the impacts of assimilating measurements of different state variables, which can be potentially available from various observational platforms, on the cycled analysis and short-range forecast of supercell thunderstorms by performing a set of observing system simulation experiments (OSSEs) using a storm-scale three-dimensional variational (3DVAR) method.

The control experiments assimilate measurements every 5 minutes for 90 minutes. It is found that the assimilation of horizontal wind ( $\vec{V}_h$ ) can reconstruct the storm fields rather accurately. The assimilation of vertical velocity ( $w$ ), potential temperature ( $\theta$ ), or water vapor ( $q_v$ ) can partially rebuild the thermodynamic and precipitation fields but poorly retrieves the wind fields. The assimilation of rain water ( $q_r$ ) can build up the precipitation fields together with a reasonable cold pool but is unable to properly recover the wind fields. Overall,  $\vec{V}_h$  data have the greatest impact while  $q_v$  the second largest impact. The impact of  $q_r$  is the smallest.

The impact of assimilation frequency is examined by comparing results using 1, 5 or 10 minute assimilation intervals. When  $\vec{V}_h$  is assimilated every 5 or 10 minutes, the analysis quality can be further improved by the ingest of additional types of observations. When  $\vec{V}_h$  are assimilated every minute, the benefits from additional types of observations are negligible except for  $q_v$ . It is also found that for  $\vec{V}_h$ ,  $w$ , and  $q_r$  measurements, more frequent assimilation leads to more accurate analyses. For  $q_v$  and  $\theta$ , one minute assimilation interval does not produce better analysis than 5 minute interval.

## 1. Introduction

The numerical weather prediction (NWP) of severe thunderstorms is very important for saving lives and properties. To get a good prediction of thunderstorms, the initial condition from which a forecast starts is expected to be as accurate as possible. During the past 20 years, much research has been done to improve initial conditions for storm-scale NWP. There are generally two ways to do so. One is to develop and improve NWP models and data assimilation techniques to make best use of available observations and background information, the other is to design and deploy additional high resolution observing systems to improve the observation of the atmosphere.

Currently, Doppler radars can provide routinely one component (radial velocity) of three-dimensional wind fields in storm-scale. The horizontal wind fields can be retrieved from multiple Doppler radar velocity observations to certain accuracy if a good multiple radar coverage can be obtained. The rainfall information (rain water mixing ratio, snow water mixing ratio, hail mixing ratio) can be assumed to be derived from radar observed reflectivity (including dual-pol information), satellite imagery data and surface cloud reports. In the future, it will be expected that the vertical velocity field can be observed in high resolution by space-borne or airborne high frequency Doppler radar. The water vapor field can be derived in high resolution from next generation GOES (Geostationary Operational Environmental Satellite) observations, radar refractivity observations, and observations by dense ground-based GPS (Global Positioning System) receiver network. The temperature field can also be profiled in high resolution by next generation GOES.

As more data assimilation and observing system studies are devoted to this area, some fundamental questions remain to be answered: What are the impacts of assimilating

measurements of different state variables on storm analysis and short-range forecast? How does the model respond from cold-start to the assimilation of individual types of measurements? How long will it take to get a quality initial condition with intermittent data assimilation? Will a more frequent assimilation (rapid update) naturally yield good results?

Weygandt et al. (1999) performed experiments to study the relative importance of different data fields in a numerically simulated convective storm by withdrawing information of each model variable and then rerunning the simulation. It is found that the perturbation horizontal velocity has the greatest influence on the evolution of the simulated convective storm. Park and Droegemeier (2000) examined the sensitivities of a supercell storm to errors in model fields in the context of four-dimensional variational data assimilation. They concluded that the forecast error is most sensitive to the inaccuracy of temperature, followed by pressure and water vapor. Weygandt et al. (2002b, 2002a) conducted several sensitivity tests and found that the supercell storm simulation was greatly dependent on initial moisture fields, especially water vapor field. Sun (2005) studied the relative importance of different initial fields on the forecast of an observed supercell storm by resetting a given initial field to its base state. The result is that wind, water vapor and temperature perturbations showed largest sensitivities. Nascimento and Droegemeier (2006) examined, using an idealized bow echo convective system, the nature of dynamic adjustment that occurred after resetting a given model data field to its base state. They found that horizontal wind fields are crucial for the correct evolution of the simulation. Fabry and Sun (2010) and Fabry (2010) studied the propagation of initial condition errors in mesoscale convections under four-dimensional variational (4DVAR) data assimilation context and found that error in midlevel moisture (humidity) has the greatest impact on the quality of the forecast. Zhang et al. (2004) conducted some sensitivity tests on the observing frequency and data

coverage for convective-scale data assimilation using an Ensemble Kalman Filter (EnKF). They found that low-level observations are important for the capture of the storms and frequent observations can improve the data assimilation in the early stage (first half hour). Tong and Xue (2005) studied the impact of radial velocity and radar reflectivity on the data assimilation for an idealized supercell thunderstorm using EnKF and found that the best results are obtained when both types of data are assimilated into the model.

All the above studies contribute to our understanding of the relative importance of different state variables during the mesoscale/storm-scale data assimilation and prediction. However, because of their different context and different focus, there are differences among the conclusions of these studies. These differences call for more research on this issue. Furthermore, the model response from cold start to the ingestion of storm-scale observations, i.e. how the model fields adjust in storm-scale as a response from cold start to the assimilation of different observations, is not explicitly investigated. In the study, we will perform over dozen of idealized experiments to study the impact of assimilating measurements of different state variables on storm analysis and short-range forecast in the context of a three-dimensional variational (3DVAR) data assimilation system (details will be given in next section). Unlike the “remove” method or sensitivity method used in most previous studies (e.g. Weygandt et al. 1999; Sun 2005; Nascimento and Droegemeier 2006), we will try to examine the relative importance of different data fields by assimilating the measurements of them into the model. For all OSS data assimilation experiments, we explore whether each of them can successfully reproduce the storm structures (dynamic, thermodynamic and precipitation structures), how long it will take to get such a successful recovery and how accurate the final data assimilation results are. In the meantime, the impact of assimilation frequency will also be examined.

This paper is organized as follows. Section 2 will cover the methodology and the design of experiments, Section 3 will discuss the results from these experiments. Conclusions will be provided in Section 4.

## 2. Methodology and experimental design

### a. The 3D variational formulation

Based on Bayesian probability theory and assuming Gaussian error distributions, Lorenc (1986) derived the standard formulations of the variational data assimilation problem. A variational method tries to determine the optimal analysis by directly minimizing a cost function. The cost function of the ARPS 3DVAR system (Gao et al. 2004) is written as:

$$J(\mathbf{X}) = J_B + J_O + J_C = \frac{1}{2}(\mathbf{X} - \mathbf{X}_b)^T \mathbf{B}^{-1}(\mathbf{X} - \mathbf{X}_b) + \frac{1}{2}[H(\mathbf{X}) - \mathbf{y}_o]^T \mathbf{R}^{-1}[H(\mathbf{X}) - \mathbf{y}_o] + J_C \quad (1)$$

where  $J_B$  measures the departure of the analysis  $\mathbf{X}$  from the background  $\mathbf{X}_b$ , and is weighted by the inverse of the background error covariance matrix  $\mathbf{B}$ ;  $J_O$  measures the departure of  $H(\mathbf{X})$ , which is the projection of the analysis  $\mathbf{X}$  into observational space, from observations  $\mathbf{y}_o$  and is weighted by the inverse of the observational error covariance matrix  $\mathbf{R}$ .  $J_C$  is the penalty term or equation constraint term, which can be used to build linkages among model variables by using, e.g., the mass continuity equation, and/or a diagnostic pressure equation (Ge et al. 2012).

In this study,  $J_C$  is not included. The reason is that although the equation constraints can help spread the observation information to some unobserved model variables, it complicates the data impact problem here since this study will examine the data impact of individual model fields or their combinations as well as the model response from cold start to the ingestion of observations.

The pseudo observations are directly drawn from the model variables, so no projection or interpolation is needed. Hence, we have a simpler form of the cost function:

$$J(\mathbf{X}) = J_B + J_O = \frac{1}{2}(\mathbf{X} - \mathbf{X}_b)^T \mathbf{B}^{-1}(\mathbf{X} - \mathbf{X}_b) + \frac{1}{2}(\mathbf{X} - \mathbf{X}_o)^T \mathbf{R}^{-1}(\mathbf{X} - \mathbf{X}_o) \quad (2)$$

The goal of obtaining an analysis is to find state  $\mathbf{X}_a$ , for which  $J$  is minimized. At the minimum, the derivative of  $J$  vanishes, and  $\mathbf{X}_a$  satisfies  $\nabla J(x) = \mathbf{B}^{-1}(\mathbf{X} - \mathbf{X}_b) + \mathbf{R}^{-1}(\mathbf{X} - \mathbf{X}_o) = 0$ . In the ARPS 3DVAR system (Gao et al. 2004), the background error covariance assumes spatially homogeneous and isotropic Gaussian spatial correlations. Its actual effects are realized through recursive filters (Purser and McQuigg 1982; Hayden and Purser 1995) as described in Gao et al. (2004). The error variances for each of the state variables will be provided in next section. It is realized that this  $\mathbf{B}$  is flow independent, as is the case with most 3DVAR systems. As a result, the assimilation of the measurements of individual state variables may not be as effective as other more advanced data assimilation methods including the EnKF and 4DVAR, where the covariance  $\mathbf{B}$  is explicitly or implicitly flow dependent. In the current 3DVAR systems, dynamic consistency among the state variables is mostly achieved through model adjustment during the high-frequency assimilation cycles. Given that the main goal of this study is to investigate the relative importance of the measurements of different state variables, we hope that conclusions will not depend too much on the assimilation method.

*b. The prediction model and truth simulation*

In this study, we use simulated data from a classic May 20, 1977 Del City, Oklahoma supercell storm case (Ray et al. 1981). The Advanced Regional Prediction System (ARPS, Xue et al. 2000; Xue et al. 2001; Xue et al. 2003) is used to simulate such a deep convective storm

within a 64 x 64 x 16 km physical domain. The model grid comprises of 67 x 67 x 35 grid points. Horizontal grid spacing of 1 km and vertical grid spacing of 0.5 km are used, with the first scalar model level located at 250 m above ground level (AGL). The truth simulation is initialized from a modified real sounding plus a +4 K ellipsoidal thermal bubble centered at  $x = 48$  km,  $y = 16$  km and  $z = 1.5$  km, with radii of 10 km in the  $x$  and  $y$  directions and 1.5 km in the vertical direction. The Kessler (1969) warm rain microphysical scheme is used together with a 1.5-order turbulent kinetic energy-based subgrid parameterization. Open conditions are used at the lateral boundaries and a wave radiation condition is applied at the top boundary. Free-slip conditions are applied to the bottom boundary. The length of the truth simulation is up to three hours. A constant wind of  $u = 3 \text{ m s}^{-1}$  and  $v = 14 \text{ m s}^{-1}$  is subtracted from the observed sounding to keep the primary storm cell near the center of model grid.

The evolution of the simulated storms is similar to those documented in Xue et al. (2001) and is shown in Fig. 1. The initial convective cell strengthens over the first 20 minutes and begins to split into two cells at around 55 minutes. The right mover moves north-northeastward and tends to dominate the system and remain near the center of domain. The left mover moves northwestward and is located at the northwest corner of the domain 2 hours into the simulation.

### *c. Experimental design*

After creating the truth simulation of the tornadic thunderstorms, pseudo measurements (observations) are generated by directly taken them from the simulated model state variables. The pseudo observations are: horizontal wind ( $\overline{V}_h$ ), vertical velocity ( $w$ ), potential temperature ( $\theta$ ), water vapor mixing ration ( $q_v$ ) and rain water mixing ratio ( $q_r$ ). Gaussian noises are

added to the above data fields to model observation errors. The error standard deviations for the observations ( $\sigma_o$ ) and the background ( $\sigma_b$ ) are given in Table 1.

The pseudo observations are taken from 30 to 120 minutes of the truth simulation. The assimilation experiments start with a horizontally homogeneous background whose vertical variation is given by the same sounding used by the truth run. At the initial time, the assimilation experiments have no storm information at all. The available pseudo observations are then assimilated into the model. The model forecast runs until the next assimilation time and such assimilation cycles are repeated from 30 to 120 minutes, through a 90 minute assimilation window.

For each assimilation frequency, twelve data assimilation experiments are conducted (Table 2). Each of the first five experiments assimilates only one type of observations. These experiments are expected to disclose how the model responds to the assimilation of different types of observations and which type of observations exerts greater impact. Each of the next four experiments assimilates horizontal wind components and one more type of observations. Each of the last three experiments assimilates three wind components and one more type of observations. The goal of the latter seven experiments is to examine the impact of assimilating observations in different combinations. Each experiment will be named according to the observation types assimilated followed by the assimilation time interval, separated by an underscore. For example, experiment VhWPt\_5 assimilates  $\overline{V}_h$ ,  $w$  and  $\theta$  every 5 minutes. Note that the first letters of variable names are capitalized and  $\theta$  is replaced by “Pt”.

To evaluate the performance of different OSSEs, we compute RMS error statistics of the model variables between the experiments and the truth simulation as follows (Ge et al. 2010):

$$RMS\_V_h = \sqrt{\frac{\sum_{i=1}^N (u - u_{simu})_i^2 + \sum_{i=1}^N (v - v_{simu})_i^2}{2N}} , \quad (3)$$

and

$$RMS\_s = \sqrt{\frac{\sum_{i=1}^N (s - s_{simu})_i^2}{N}} , \quad (4)$$

where  $N$  is the total number of grid points used in the calculation,  $u$  and  $v$  are the horizontal wind components in x and y directions, respectively,  $s$  stands for scalar model variable and subscript  $simu$  stands for data from the truth simulation. In this study, we will compute the RMS error statistics for  $\vec{V}_h, w, \theta', q'_v, q'_r$ , which can be regarded as five performance indices and the time evolution of these indices can be used to illustrate how different model fields change during the assimilation process.

To make the performance evaluation more convenient, we follow Fabry and Sun (2010) to compute the so-called ‘‘energy difference (ED)’’ between the experiments and the truth simulation. Three types of ED’s are defined here, i.e., the kinetic energy difference (KED), the thermal energy difference (TED), and the latent energy difference (LED):

$$KED = \frac{1}{2} \int_D (\Delta u^2 + \Delta v^2 + \Delta w^2) dD , \quad (5)$$

and

$$TED = \frac{c_p}{2T_r} \int_D \Delta T^2 dD , \quad (6)$$

and

$$LED = \frac{L^2}{2c_p T_r} \int_D \Delta q_v^2 dD , \quad (7)$$

where  $D$  stands for the integration domain,  $\Delta(\dots)$  means to calculate the difference,  $c_p$  is the specific heat,  $T_r$  is the reference temperature and  $T_r = 270$  K following Ehrendorfer and Errico (1995), and  $L$  is the latent heat of vaporization. In their paper, Fabry and Sun (2010) computed the summation of all ED terms. Similarly, we computed the summation of KED, TED and LED but found that KED dominates the sum. This means that the summation of all ED's represents mostly errors in the dynamic features while representing thermodynamic and precipitation structures less prominently. Therefore the summation of all ED terms is not very effective for evaluating and delineating the experiments and we introduce the scaled ED's, i.e., SKED, STED, SLED, which are computed by dividing the ED's by their corresponding values at the beginning of data assimilation window. The average of the three scaled ED's (ASED) is then used as an index to evaluate the accuracy of analyzed storms.

For hydrometeors, it is hard to find an "ED" similar to those described above. In this study, we elected to use the RMS error in simulated reflectivity (RMSZ) to evaluate the difference in rain water mixing ratio between the experiments and the truth simulation. This index is straightforward since the simulated reflectivity directly shows the location, shape and structure of the storms. Using both ASED and RMSZ, we can now conveniently compare the performance of different assimilation experiments.

To measure how fast different experiments successfully recover the simulated storms, a "successfully recovery time (SRT)" is defined as the length it takes for an experiment to meet the criteria that each of its scaled ED's is less than 0.2 and that RMSZ is less than 10 dBZ. To measure how accurate the recovered storms are at the end of data assimilation, ASED and RMSZ at the final analysis time are computed and compared among different experiments.

It should be noted that when calculating the RMS errors and ED's, only grid points which are located in the cloudy regions, defined as regions where simulated reflectivity  $\geq 10\text{dBz}$ , are included.

### **3. Results of experiments**

In this study, twelve data assimilation experiments are conducted for each assimilation frequency (every minute, five minutes, or ten minutes). Hence, there are a total of thirty six data assimilation experiments. For each experiment, the SRT, final ASER, and final RMSZ are determined according to the criteria described in previous section and listed in Table 2. A blank will be left for those experiments that do not reach “successful recovery” at the end of assimilation window.

#### *a. Experiments assimilating one type of observations*

The experiments assimilating one type of observations are suitable for investigating the model responses from cold start to the assimilation of individual type of observations. In these experiments, from the analysis of the first cycle (i.e., at the beginning of data assimilation window), a five-minute-long forecast is launched and the forecasting results are output every time step (every 6 seconds in this study) to allow for close examinations. In the following subsections 1) ~ 5), we will focus on the model responses from cold start to different types of observations; in subsection 6), the impacts of different types of observations will be addressed and compared. The section focus on experiments that assimilate observations every five minutes. Results with lower and higher assimilation frequencies will be discussed in later sections.

## 1) Assimilating horizontal winds

When both horizontal wind components are assimilated, the model fields that are affected most in the first five minutes are the vertical velocity, potential temperature and water vapor mixing ratio. As an example, Fig. 2 shows horizontal wind divergence (DIV), vertical velocity ( $w$ ), perturbation potential temperature ( $\theta'$ ) and perturbation water vapor mixing ratio ( $q'_v$ ) from experiment Vh\_5 at  $t = 0$  s, 6 s, 12 s, 300 s into the assimilation run at 4 km above ground. It can be seen that at  $t = 0$  s, the ingestion of horizontal wind observations produces horizontal wind divergence/convergence (Fig. 2a) while  $w$ ,  $\theta'$  and  $q'_v$  remain unchanged (Fig. 2b, c, d). After one integration time step at  $t = 6$  s, DIV decreases (Fig. 2e vs. Fig. 2a). At the same time, an updraft center with a maximum value of  $6.277 \text{ m s}^{-1}$  and a couple of downdraft centers appear in the  $w$  field (Fig. 2f). The updraft/downdraft centers are co-located with convergence/divergence centers shown in Fig. 2a. There is barely any change in  $\theta'$  and  $q'_v$  fields at this moment (Fig. 2g, h). Six more seconds later ( $t = 12$  s), weak perturbations start to appear in  $\theta'$  and  $q'_v$  fields (Fig. 2k, l). As the model integrates forward further,  $\theta'$  and  $q'_v$  further increase and become more organized while DIV and  $w$  decrease and become less organized (Fig. 2o, p vs. Fig. 2m, n).

Therefore, it is clear that the model response from cold start to the assimilation of horizontal wind observations is to produce horizontal wind convergence/divergence. Updrafts and downdrafts are then induced by the convergence/divergence in updated horizontal wind fields. After that, the established vertical air movement perturbs the potential temperature and water vapor fields, which are horizontally homogeneous before. As the model integrates forward, the magnitudes of perturbation horizontal winds and vertical velocity decrease while those of perturbation water vapor and perturbation potential temperature fields increase.

Such data impact is reinforced as new horizontal wind observations are assimilated into the model in subsequent data assimilation cycles. The adjustments in dynamic fields and thermodynamic fields will eventually induce convection and precipitation.

Fig. 3 shows the perturbation horizontal winds, perturbation potential temperature, and reflectivity fields at  $z = 250$  m AGL and the perturbation horizontal winds, vertical velocity, perturbation water vapor fields at 5 km height every thirty minutes from 20 to 80 minutes into the assimilation window ( corresponding to 50 to 110 minutes of the truth simulation). It is clear that after four assimilation cycles (20 minutes into the assimilation), small areas of precipitation has been produced (Fig. 3a). The vertical velocity and water vapor fields have also been partially re-constructed (Fig. 3d). As the assimilation cycles continue, the precipitation becomes stronger and spreads to wider areas (Fig. 3b). The vertical velocity and perturbation water vapor fields become closer to those of truth simulation (Fig. 3e vs. Fig. 1e). After 80 minutes of assimilation, recovered storm cells are very close to those of truth (Fig. 3c, f). Actually, according to our SRT criterion, 70 minutes into the assimilation, the dynamic, thermodynamic and precipitation structures of the storms have already been successfully reconstructed.

We also conducted supplemental experiments (not shown) that assimilate measurements of only one of the horizontal wind components ( $u$  or  $v$ ). It is found that the model response from cold-start to  $u$  or  $v$  observations is kind of similar to the assimilation of both horizontal wind components. However, the magnitude of response is much smaller and assimilating only one component cannot successfully recover storm structures after 90 minutes of intermittent data assimilation. This may be related to the limited ability of the 3DVAR to directly ‘retrieve’ non-observed wind component when only one component is measured, and more advanced methods such as the 4DVAR may be able to do better.

## 2) Assimilating vertical velocity

When  $w$  observations are assimilated into the model at the first assimilation cycle, the model response from cold-start is also investigated carefully. It is found that (figures not shown) after  $w$  observations are assimilated into the model, other model fields will be perturbed by the upward or downward advection as model integrates forward. Warm moist air in the low level is then brought upward. When saturation is reached, condensation occurs. Other dynamic and thermodynamic fields in the model adjust accordingly. The data impact is reinforced through the following data assimilation cycles.

Fig. 4 shows the perturbation horizontal winds, perturbation potential temperature, and reflectivity at 250 m height, and the perturbation horizontal winds, vertical velocity, perturbation water vapor fields at 5 km height every thirty minutes from 20 to 80 minutes into the assimilation (corresponding to 50 to 110 minutes of truth simulation time). It can be seen that in terms of reflectivity, the storm cell near the center of domain is reasonably recovered near the end of the assimilation window (Fig. 4c, f). The storm cell at the upper-left corner is also partially rebuilt.

On the other hand, noticeable discrepancies still exist in the horizontal winds (Fig. 4c, f), perturbation potential temperature (Fig. 4c) and perturbation water vapor (Fig. 4f) fields. Further, the reflectivity pattern is not close enough to that in the truth. According the SRT criterion, this experiment fails to successfully recover the simulated thunderstorms.

## 3) Assimilating potential temperature

When  $\theta$  observations are assimilated, its direct impact on the model is to change the buoyancy, which in turn promotes vertical motion. The horizontal wind and water vapor fields then change accordingly. Rainfall is produced gradually with continued assimilation cycles.

As before, Fig. 5 shows the perturbation horizontal winds, perturbation potential temperature, and reflectivity at  $z = 250$  m AGL and the perturbation horizontal wind, vertical velocity, and perturbation water vapor fields at  $z = 5$  km AGL every thirty minutes from 20 to 80 minutes into the assimilation. Near the end of assimilation window, the recovered reflectivity (Fig. 5c) is comparable to those in the truth (Fig. 1c). Two storm cells are located at the correct locations with right strengths. However, the areas with reflectivity value between 15 dBZ – 25 dBZ are still evidently different from those in the truth run. Much difference also exists in the mid-upper wind and water vapor fields (Fig. 5f) as compared to the truth simulation (Fig. 1f).

Fig. 6 presents the evolution of RMS error statistics from experiment Pt\_5. It clearly shows that the impact of assimilating  $\theta$  observations is mostly on recovering the storm precipitation structure. The vertical velocity field is only partially rebuilt. The horizontal wind and water vapor fields are poorly retrieved. Overall, this experiment also fails to successfully recover the simulated thunderstorms after 90 minutes of intermittent data assimilation.

#### 4) Assimilating water vapor

When  $q_v$  observations are assimilated into the model at the beginning of data assimilation window, the main response from the model is to produce cloud water (Fig. 7h) through condensation which heats the air (Fig. 7f). The change to the buoyancy due to water vapor perturbation is another cause of model response but this effect is much smaller. This can be confirmed by Fig. 7g, which shows little change in the vertical velocity. Detailed scale analysis (not shown here) for the buoyancy terms indicates that the contribution of perturbation water vapor to the buoyancy is on the order of  $0.01 \text{ m s}^{-2}$  near storm center while the contribution of perturbation potential temperature is on the order of  $0.1 \text{ m s}^{-2}$ . Therefore, the direct buoyancy response from the assimilation of  $q_v$  observations is rather small compared to the impact of

induced condensation and associated latent heating. The changed temperature will then induce vertical motion as seen in the  $w$  field (Fig. 7k), which is six more seconds later at  $t = 12$  s. As the model continues to integrate forward, more condensation and latent heating are produced (Fig. 7n, p) and  $w$  also increases in magnitude.

The recovery of reflectivity goes very well in this experiment as shown in Fig. 8. As early as at 50 minutes (Fig. 8b) into the assimilation, the reflectivity pattern has become very comparable to that of truth. Near the end of assimilation window (Fig. 8c), the reflectivity pattern is much closer to the truth. The final RMS error for simulated reflectivity at 90 minutes into the assimilation is 7.3 dBZ, below the 10 dBZ error level set by the SRT criterion. The recovery of temperature field also goes well. Fig. 8c shows that the cold pool is reasonably re-established around both storm cells. The location and coverage are reasonable compared to those in the truth simulation. On the other hand, the wind fields (Fig. 8f), especially the horizontal wind fields are poorly recovered. This can also be seen from Fig. 9, where the decrease in the RMS errors for horizontal winds is very limited. Therefore, on the whole, this experiment is still considered as failing to successfully recover the simulated thunderstorms.

#### 5) Assimilating rain water

When  $q_r$  observations are assimilated, its major impact on the model is to change the buoyancy through water loading and therefore to produce downward vertical motion (Fig. 10e, h). Evaporative cooling is another noticeable impact (Fig. 10f, i), which also tends to induce downdraft. The wind and water vapor fields will then adjust in response to these processes.

With continued intermittent data assimilation, the cold pool is rebuilt well (Fig. 11b, c) although there still exists noticeable differences in its strength and distribution. However, the mid-upper level temperature field (not shown) is not retrieved well and the wind and water vapor

fields (Fig. 11c, f) are barely recovered. This experiment also fails to successfully recover the simulated thunderstorms.

## 6) Summary

When individually assimilating one type of observations every five minutes, only experiment Vh\_5 can successfully recover the simulated thunderstorms with SRT = 70 minutes (see Table 2). At the end of the data assimilation window, Vh\_5 yields a very low ASED (0.067) and RMSZ (4.1 dBZ), much smaller than those of experiments W\_5, Pt\_5, Qv\_5 and Qr\_5. These results indicate that the assimilation of horizontal wind components have the largest impact on the supercell storm analysis and short-range forecast. This conclusion is consistent with the findings of Weygandt et al. (1999), Sun (2005), and Nascimento and Droegemeier (2006).

Among experiments W\_5, Pt\_5, Qv\_5 and Qr\_5 that assimilate  $w, \theta, q_v, q_r$  data individually without horizontal winds, Qv\_5 yields the smallest ASED (0.371) and RMSZ (7.3 dBZ). Therefore, water vapor is the second most important type of observation. A similar conclusion was drawn in Sun (2005). Weygandt et al. (2002b, 2002a) also indicate that a supercell storm simulation is greatly affected by the water vapor field. The  $q_v$  observations are very effective in rebuilding precipitation field and, to some extent, thermodynamic fields but they are poor at recovering wind fields. The  $w$  observations have the third most important impact given that experiment W\_5 produces smaller ASED and RMSZ than Pt\_5 and Qr\_5 do. The  $q_r$  observations have the least impact; they perform poorly at recovering either the dynamic or thermodynamic structures.

*b. Experiments assimilating horizontal wind components and one more type of observations*

Experiment Vh\_5 yields a SRT of 70 minutes (Table 2), indicating the effectiveness of assimilating horizontal wind components. On the other hand, it still takes the experiment seventy minutes to reach a successful-recovery, which is quite long considering the life cycle of typical convective storms and the operational need of quick delivery of storm-scale forecasts.

Assimilating one more type of observations may help alleviate this problem. As seen in Table 2, VhW\_5 has a SRT of 36 minutes, VhPt\_5 28 minutes, VhQv\_5 18 minutes, and VhQr 46 minutes. All of these SRT's are much smaller than the 70 minutes of Vh\_5. Therefore, it confirms that one more type of observations in addition to horizontal wind can accelerate the "successful-recovery" of simulated storms, when measurements are assimilated every 5 minutes. Similar behaviors were also found in Tong and Xue (2005), Hu et al. (2006), Zhao and Xue (2009), where the assimilation of radar reflectivity data in addition to radial velocity data was found to improve the data assimilation results.

Among VhW\_5, VhPt\_5, VhQv\_5 and VhQr\_5, experiment VhQv\_5 yields the smallest SRT (28 minutes). This confirms again that water vapor measurements are the second most important type of observations after horizontal wind measurements. It can also be seen that with the availability of horizontal winds, additional  $\theta$  observations make the storms recover faster than additional  $w$  observations (SRT of 28 minutes for VhPt\_5 vs. 36 minutes for VhW\_5). The behavior that temperature observations add more useful information to the analysis can be attributed to the fact that the vertical velocity is more closely correlated to the horizontal wind divergence than temperature therefore the latter offers more independent information.

Experiment VhQr\_5 yields the largest SRT of 46 minutes among VhW\_5, VhPt\_5, VhQv\_5, and VhQr\_5. This further confirms that  $q_r$  gives the least impact compared to  $q_v, w$  and  $\theta$  observations.

*c. Experiments assimilating all three wind components and one more type of observations*

The experiment that assimilates all three wind components yields a SRT of 36 minutes, which is much smaller than when assimilating only the horizontal wind components (Vh\_5 has an SRT of 70 minutes). This indicates that for storm-scale data assimilation, most efforts should be made in getting as accurate three wind components as possible. In practice, this can be achieved through the measurements and assimilation of radial velocity data from multiple Doppler radars. Schenkman et al (2011) showed that assimilating multiple CASA (Center for Collaborative and Adaptive Sensing of the Atmosphere) radar radial velocity data in addition to WSR-88D radar data improves the forecasting of a mesoscale convective system. The finding also suggests that importance of further developing advanced velocity retrieval schemes from single or multiple Doppler radar data. For example, Shapiro et al (2009) reported that including a vorticity equation constraint in a 3D variational framework could improve dual-Doppler wind analysis.

Experiments VhWPt\_5, VhWQv\_5, and VhWQr\_5 all perform better than VhW\_5 as the former three have much smaller SRT's than the latter. It means that assimilating one more type of observations in addition to the three wind components can further improve data assimilation results. Among those three experiments, VhWQv\_5 has the smallest SRT value and VhWQr\_5 the largest one. This, once again, confirms that after the horizontal wind measurements, water vapor is the second most important type of observation and  $q_r$  is the least important one.

*d. The impact of assimilation frequency*

In Table 2, the experiments assimilating observations every 5 minutes all have smaller SRT's than the corresponding experiments assimilating the same types of observations every 10 minutes. The better performance with a five minute interval is obviously due to the assimilation of more observations. When model variables are updated more frequently, the model state variables are impacted more by the observations and the data impact are usually better maintained and the model storms are recovered in a shorter amount of time. This finding is consistent with those of Zhang et al. (2004), Xue et al. (2006), and Hu and Xue (2007), which also examined, using EnKF or 3DVAR method, the assimilation frequency on the analysis of convective storms.

The above statements naturally lead to a question: since a higher assimilation frequency can produce better results, can we assimilate observations at the highest frequency possible (e.g., every model time step if such data are available) in order to obtain better analyses? It is not necessarily so in practice. From Fig. 12 and Table 2, it can be seen that assimilating observations every minute does not show obvious improvement over assimilating observations every five minutes. The SRT's of VhWQv\_1 and VhWQr\_1 are only 2 minutes shorter than the corresponding values of VhWQv\_5 and VhWQr\_5. Such small improvement is not worth it compared to the much increased computational and data collection costs. At the same time, VhPt\_1 and VhWPt\_1 actually give somewhat larger SRT's than VhPt\_5 and VhWPt\_5. Further examinations show that this is because VhPt\_1 and VhWPt\_1 generally produce larger LED values, whose computation is based on the water vapor field, than VhPt\_5 and VhWPt\_5. We attribute this behavior to the following: the pseudo potential temperature measurements are assumed to be available at the grid points and they contain added random noise. When

assimilated into the model at high frequency, the increased noise level can have negative impact on the precipitation forecast. The model needs some time to adjust and damp out such noise. One minute model integration may be too short for the model to completely remove the noise. These results suggest that in some situations (as with temperature measurements in this case), the assimilation of observations at too high a frequency may hurt the analysis. On the other hand, experiments assimilating Vh, W, VhW observations every minute show benefits of a higher frequency, suggesting that it is generally beneficial to assimilate wind observations at high frequency.

It is already shown in section 3.b that one more type of observations in addition to horizontal wind components can accelerate the “successful-recovery” of simulated storms when measurements are assimilated every 5 minutes. The same conclusion can be drawn when assimilating data every 10 minutes (see Table 2). However, when assimilating observations every minute, the SRT’s from VhW\_1, VhPt\_1 and VhQr\_1 are not much reduced compared to Vh\_1. The ASER’s and RMSZ’s from those three experiments increase slightly compared to Vh\_1. At the same time, the SRT of VhQv\_1 is smaller than that of Vh\_1. Therefore, when assimilating horizontal wind observations every minute, the benefits from one more type of observations are not evident except for water vapor observations. This is presumably because assimilating wind observations at one minute interval is already very effectively at building up the model storm; additional help from additional measurements has only small effect. This is even true when all three wind components are assimilated; in that case, little additional improvement is obtained when the three wind components are already assimilated at 1 minute interval.

#### **4. Summary and conclusions**

An as accurate initial condition as possible is very important for making quality storm-scale NWP of thunderstorms. Many efforts have been made to obtain better initial conditions for storm-scale NWP. Some focus on developing and improving NWP model and data assimilation techniques to make best use of available observations and background information. Others try to design and implement higher resolution observing systems to provide measurements of more variables. Despite all these efforts, a clear understanding of the impacts of assimilating measurements of different state variables on storm analysis and short-range forecasting is still lacking.

In this study, we examined the impacts of assimilating measurements of different state variables as well as the impacts of data assimilation frequency through a series of OSS experiments using a three-dimensional variational data assimilation method. Different types of pseudo observations are assimilated into a storm-scale NWP model individually or in combinations. The model responses from cold-start to the assimilation of individual types of observations are investigated in detail to help us understand the impact of the observations. Term “successful-recovery” is defined using the energy difference and the RMS error of simulated reflectivity between the assimilation run and truth run. It defines the criterion when the dynamic, thermodynamic and precipitation structures of the storm in the assimilation run are analyzed to be close enough to the truth simulation. This criterion is then used to evaluate the performance of different data assimilation experiments so that the impacts of different types of observations and assimilation frequencies can be quantified.

It is found that the model responses from cold start to the assimilation of horizontal wind observations is to force vertical motions through horizontal wind divergence/convergence which

in turn forces temperature and humidity perturbations through upward and downward motions. With continuing intermittent data assimilation cycles, storm dynamic and thermodynamic structures are spun-up gradually. When vertical velocity observations are assimilated, other model variables are directly perturbed by the upward and downward advection. Temperature, humidity and precipitation fields can then be recovered to some extent in ensuing assimilation cycles but the horizontal wind components are barely rebuilt in this case. When potential temperature observations are assimilated, the direct adjustment in the model is the change to air buoyancy, which induces vertical air motion. Precipitation fields can be spun-up to some extent but the horizontal wind, vertical velocity and humidity fields are retrieved very poorly. When the model ingests water vapor observations, its main response is to produce cloud water through condensation and heat the air through latent heat release. The changed temperature will then promote vertical motion. This makes water vapor observations effective at reconstructing temperature, precipitation and, to some extent, vertical velocity fields, but ineffective at recovering horizontal winds. As to rain water observations, its impact is to change air buoyancy through water loading and through evaporative cooling and hence the main direct effect is to produce downward motion. The rain water observations perform well in quickly reproducing precipitation field and constructing a reasonable cold pool but are poor at rebuilding storm dynamic and thermodynamic structures.

Among all types of measurements, horizontal wind observations have the greatest impact on storm analysis and short-range forecast. It is so because the assimilation of horizontal wind observations is very effective at recovering other model fields. Therefore, in practice, great efforts should be made to obtain as many and as accurate wind observations as possible.

The impact of water vapor observations is the second largest. Currently, to get storm-scale water vapor observations is a difficult task. However, some of water vapor information can be derived from near-surface refractivity measurements by radars (Fabry et al. 1997; Bodine et al. 2010). Such data can be assimilated into the model (Gasperoni et al. 2012). In the future, water vapor information may be available at high resolution due to the advances in the observing systems such as next generation GOES satellite, dense ground-based GPS receiver network (Wolfe and Gutman 2000; Liu and Xue 2006; Ho et al. 2007; Liu et al. 2007). The assimilation of such dense observations is expected to significantly improve storm-scale NWP.

The relative importance of vertical velocity and potential temperature measurements is somewhat dependent on data assimilation frequency. When assimilating data every minute, vertical velocity observations exert larger impact than potential temperature observations. On the other hand, when assimilated every 5 or 10 minutes, potential temperature observations are more effective than vertical velocity observations. Rain water observations show the least impact.

The impact of data assimilation frequency is also examined. In general, the assimilation frequency has an important effect on the quality of convective storm analysis. In this study, results with 1, 5 and 10 minute assimilation intervals are compared. When assimilating horizontal wind observations every 5 or 10 minutes, additional types of observations will improve the analysis and subsequent short-range forecast. However, when the horizontal wind observations or all three wind components are assimilated every minute, the benefits from additional observation types become negligible except for water vapor measurements. This is apparently because the results from assimilating the wind components at such a high frequency are already very good; additional observations do not lend much further help. It is also found that for measurements of horizontal wind, vertical velocity, rain water or their combinations, 1

minute assimilation frequency produces the best results. For measurements of potential temperature, water vapor or their combinations with winds, 1 minute data assimilation frequency does not produce better analysis than 5 minute frequency. The time needed for the model to adjust and damp out noise introduced by the frequent assimilation is believed to be the cause.

While the above findings can provide guidance to the design /improvement of storm-scale observing systems and storm-scale data assimilation practice, it should be noted that the conclusions obtained here are based on a single idealized supercell storm using a particular data assimilation method. Whether the conclusions apply to other cases, and when using other data assimilation methods will require further study.

***Acknowledgments.*** This research was supported by NSF grants ATM-0738370, ATM-0802888 and NOAA's Warn-on-Forecast project. Computations were performed at the Pittsburgh Supercomputing Center (PSC) and Oklahoma Supercomputing Center for Research and Education (OSCER). The third author acknowledges the support of NSF grants, OCI-0905040, AGS-0941491, AGS-1046171, and AGS-1046081, and National 973 Fundamental Research Program of China (2013CB430103). Thoughtful comments from two anonymous reviewers and Editor Dr. Fuqing Zhang significantly improved this paper.

## References

- Bodine, D., P. L. Heinselman, B. L. Cheong, R. D. Palmer, and D. Michaud, 2010: A Case Study on the Impact of Moisture Variability on Convection Initiation Using Radar Refractivity Retrievals. *J. Appl. Meteor. Climatol.*, **49**, 1766-1778.
- Ehrendorfer, M., and R. M. Errico, 1995: Mesoscale predictability and the spectrum of optimal perturbations. *J. Atmos. Sci.*, **52**, 3475-3500.
- Fabry, F., 2010: For how long should what data be assimilated for the mesoscale forecasting of convection and why? Part II: On the observation signal from different sensors. *Mon. Wea. Rev.*, **138**, 256-264.
- Fabry, F., and J. Sun, 2010: For how long should what data be assimilated for the Mesoscale forecasting of convection and why? Part I: On the propagation of initial condition errors and their implications for data assimilation. *Mon. Wea. Rev.*, **138**, 242-255.
- Fabry, F., C. Frush, I. Zawadzki, and A. Kilambi, 1997: On the extraction of near-surface index of refraction using radar phase measurements from ground targets. *J. Atmos. Oceanic Technol.*, **14**, 978-987.
- Gao, J.-D., M. Xue, K. Brewster, and K. K. Droegemeier, 2004: A three-dimensional variational data analysis method with recursive filter for Doppler radars. *J. Atmos. Ocean. Tech.*, **21**, 457-469.
- Gasperoni, N. A., M. Xue, R. D. Palmer, and J. Gao, 2012: Sensitivity of convective initiation prediction to near-surface moisture when assimilating radar refractivity: Impact tests using OSSEs. *J. Atmos. Ocean Tech.*, **Conditionally accepted**.

- Ge, G., J. Gao, and M. Xue, 2012: Diagnostic Pressure Equation as a Weak Constraint in a Storm-Scale Three Dimensional Variational Radar Data Assimilation System. *J. Atmos. Oceanic. Technol.*, **29**, 1075-1092.
- Ge, G., J. Gao, K. Brewster, and M. Xue, 2010: Impacts of beam broadening and earth curvature on Storm-Scale 3D variational data assimilation of radial velocity with two Doppler radars. *J. Atmos. Oceanic. Technol.*, **27**, 617-636.
- Hayden, C. M., and R. J. Purser, 1995: Recursive filter objective analysis of meteorological fields: applications to NESDIS operational processing. *J. Appl. Meteor.*, **34**, 3-15.
- Ho, S., Y. Kuo, and S. Sokolovskiy, 2007: Improvement of the Temperature and Moisture Retrievals in the Lower Troposphere Using AIRS and GPS Radio Occultation Measurements. *J. Atmos. Oceanic. Technol.*, **24**, 1726-1739.
- Hu, M., and M. Xue, 2007: Impact of configurations of rapid intermittent assimilation of WSR-88D radar data for the 8 May 2003 Oklahoma City tornadic thunderstorm case. *Mon. Wea. Rev.*, **135**, 507-525.
- Hu, M., M. Xue, J. Gao, and K. Brewster, 2006: 3DVAR and cloud analysis with WSR-88D level-II data for the prediction of Fort Worth tornadic thunderstorms. Part II: Impact of radial velocity analysis via 3DVAR. *Mon. Wea. Rev.*, **134**, 699-721.
- Kessler, E., 1969: On the Distribution and Continuity of Water Substance in Atmospheric Circulations. *Meteor. Monogr.*, **No. 32**, Amer. Meteor. Soc., 84pp.
- Liu, H., and M. Xue, 2006: Retrieval of moisture from slant-path water vapor observations of a hypothetical GPS network using a three-dimensional variational scheme with anisotropic background error. *Mon. Wea. Rev.*, **134**, 933-949.

- Liu, H., M. Xue, R. J. Purser, and D. F. Parrish, 2007: Retrieval of moisture from simulated GPS slant-path water vapor observations using 3DVAR with anisotropic recursive filters. *Mon. Wea. Rev.*, **135**, 1506–1521.
- Lorenc, A. C., 1986: Analysis methods for numerical weather prediction. *Quart. J. Roy. Meteor. Soc.*, **112**, 1177-1194.
- Nascimento, E. L., and K. K. Droegemeier, 2006: Dynamic Adjustment in a Numerically Simulated Mesoscale Convective System: Impact of the Velocity Field. *J. Atmos. Sci.*, **63**, 2246-2268.
- Park, S. K., and K. K. Droegemeier, 2000: Sensitivity analysis of a 3D convective storm: Implications for variational data assimilation and forecast error. *Mon. Wea. Rev.*, **128**, 140-159.
- Purser, R. J., and R. McQuigg, 1982: A successive correction analysis scheme using recursive numerical filters. Met. O 11 Tech. Note, No. 154, British Meteorological Office, 17 pp.
- Ray, P. S., and Coauthors, 1981: The morphology of severe tornadic storms on 20 May 1977. *J. Atmos. Sci.*, **38**, 1643-1663.
- Schenkman, A. D., M. Xue, A. Shapiro, K. Brewster, and J. Gao, 2011: The Analysis and Prediction of the 8–9 May 2007 Oklahoma Tornadic Mesoscale Convective System by Assimilating WSR-88D and CASA Radar Data using 3DVAR. *Mon. Wea. Rev.*, **139**, 224-246.
- Shapiro, A., C. K. Potvin, and J. Gao, 2009: Use of a mesoscale vertical vorticity in variational dual-Doppler wind analysis. *J. Atmos. Oceanic. Technol.*, **26**, 2089-2106.
- Sun, J., 2005: Initialization and numerical forecasting of a supercell storm observed during STEPS. *Mon. Wea. Rev.*, **133**, 793-813.

- Tong, M., and M. Xue, 2005: Ensemble Kalman filter assimilation of Doppler radar data with a compressible nonhydrostatic model: OSS Experiments. *Mon. Wea. Rev.*, **133**, 1789-1807.
- Weygandt, S., P. Nutter, K. E. P. S., and K. Droegemeier, 1999: The relative importance of different data fields in a numerically simulated convective storm. *The 8th Conference on Mesoscale Processes, Amer. Meteor. Soc.*, Boulder, CO., American Meteorological Society, Boston, USA, 310-315.
- Weygandt, S. S., A. Shapiro, and K. K. Droegemeier, 2002a: Retrieval of model initial fields from single-Doppler observations of a supercell thunderstorm. Part II: Thermodynamic retrieval and numerical prediction. *Mon. Wea. Rev.*, **130**, 454-476.
- , 2002b: Retrieval of Model Initial Fields from Single-Doppler Observations of a Supercell Thunderstorm. Part I: Single-Doppler Velocity Retrieval. *Mon. Wea. Rev.*, **130**, 433-453.
- Wolfe, D. E., and S. I. Gutman, 2000: Developing an Operational, Surface-Based, GPS, Water Vapor Observing System for NOAA: Network Design and Results. *J. Atmos. Oceanic Technol.*, **17**, 426-440.
- Xue, M., K. K. Droegemeier, and V. Wong, 2000: The Advanced Regional Prediction System (ARPS) - A multiscale nonhydrostatic atmospheric simulation and prediction tool. Part I: Model dynamics and verification. *Meteor. Atmos. Phys.*, **75**, 161-193.
- Xue, M., M. Tong, and K. K. Droegemeier, 2006: An OSSE framework based on the ensemble square-root Kalman filter for evaluating impact of data from radar networks on thunderstorm analysis and forecast. *J. Atmos. Ocean Tech.*, **23**, 46-66.
- Xue, M., D. Wang, J. Gao, K. Brewster, and K. K. Droegemeier, 2003: The Advanced Regional Prediction System (ARPS), storm-scale numerical weather prediction and data assimilation. *Meteor. Atmos. Phys.*, **82**, 139-170.

- Xue, M., and Coauthors, 2001: The Advanced Regional Prediction System (ARPS) - A multi-scale nonhydrostatic atmospheric simulation and prediction tool. Part II: Model physics and applications. *Meteor. Atmos. Phys.*, **76**, 143-166.
- Zhang, F., C. Snyder, and J. Sun, 2004: Impacts of initial estimate and observations on the convective-scale data assimilation with an ensemble Kalman filter. *Mon. Wea. Rev.*, **132**, 1238-1253.
- Zhao, K., and M. Xue, 2009: Assimilation of coastal Doppler radar data with the ARPS 3DVAR and cloud analysis for the prediction of Hurricane Ike (2008). *Geophys. Res. Lett.*, doi:10.1029/2009GL038658.

**Table captions**

Table 1. Standard deviations of observation error ( $\sigma_o$ ) and background error ( $\sigma_b$ )

Table 2. The list of experiments assimilating measurements, their corresponding SRT (minutes), ASED and RMSZ (dBZ) at the end of 90 minutes data assimilation.

## Figure captions

Fig. 1. (a), (b) and (c):  $Vh'$  (vectors),  $\theta'$  (contours every 1 K) and reflectivity (shaded) at  $z = 250$  m AGL; (d), (e) and (f):  $Vh'$  (vectors),  $w$  (contours every  $6 \text{ m s}^{-1}$ ) and  $qv'$  (shaded) at  $z = 5$  km AGL from the simulation run every 30 minutes from 50 to 110 minutes into the truth simulation. (a) and (d)  $t = 50$  min, (b) and (e)  $t = 80$  min, (c) and (f)  $t = 110$  min.

Fig. 2. The horizontal wind divergence field, vertical velocity, perturbation potential temperature, perturbation water vapor mixing ratio for experiment  $Vh\_5$  at  $z = 4$  km AGL. (a),(b),(c),(d) are at  $t = 0$  s into the assimilation run; (e), (f), (g), (h) are at  $t = 6$  s into the assimilation run, (i),(j),(k),(l) are at  $t = 12$  s into the assimilation run; (m),(n),(o),(p) are at  $t = 300$  s into the assimilation run. (k) and (l) use different contour intervals to (o) and (p). The horizontal axis starts from 20 km and the vertical axis starts from 10 km.

Fig. 3. (a), (b) and (c):  $Vh'$  (vectors),  $\theta'$  (contours every 1 K) and reflectivity (shaded) at  $z = 250$  m AGL; (d), (e) and (f):  $Vh'$  (vectors),  $w$  (contours every  $6 \text{ m s}^{-1}$ ) and  $qv'$  (shaded) at  $z = 5$  km AGL for experiment  $Vh\_5$  experiment every 30 minutes from 20 to 80 minutes into the assimilation run (corresponding to 50 to 110 minutes into truth simulation). (a) and (d)  $t = 20$  min, (b) and (e)  $t = 50$  min, (c) and (f)  $t = 80$  min.

Fig. 4. Similar to Fig. 3, but for experiment  $W\_5$ .

Fig. 5. Similar to Fig. 3, but for the experiment  $Pt\_5$ .

Fig. 6. The RMS errors of analyses (at 5 minute intervals) and of forecasts every minute for experiment  $Pt\_5$ . The horizontal axis shows the minutes into the truth run.

Fig. 7. The perturbation water vapor mixing ratio, perturbation potential temperature, vertical velocity, cloud water mixing ratio for experiment  $Qv\_5$  at  $z = 4$  km AGL. (a),(b),(c),(d) are at  $t = 0$  s into the assimilation run; (e),(f),(g),(h) are at  $t = 6$  s into the assimilation run,

(i),(j),(k),(l) are at  $t = 12$  s into the assimilation run; (m),(n),(o),(p) are at  $t = 300$  s into the assimilation run. The horizontal axis starts from 20 km and the vertical axis starts from 10 km.

Fig. 8. Similar to Fig. 3, but for experiment Qv\_5.

Fig. 9. The RMS errors of analyses (at 5 minute intervals) and of forecasts every minute for experiment Qv\_5. The horizontal axis shows the minutes into the truth run.

Fig. 10. The rainwater mixing ratio, vertical velocity, perturbation potential temperature from experiment Qr\_5, at  $z = 4$  km AGL. (a),(b),(c) are at  $t = 0$  s into the assimilation run; (d),(e),(f) are at  $t = 6$  s into the assimilation run, (g),(h),(i) are at  $t = 12$  s into the assimilation run. The horizontal axis starts from 20 km and the vertical axis starts from 10 km.

Fig. 11. Similar to Fig. 3, but for experiment Qr\_5.

Fig. 12. Bar chart of the SRT values from experiments assimilating two- and three-types of measurements. The vertical axis shows the SRT values in unit of minutes; the horizontal axis shows different observation combinations. For each observation combination, three bars are plotted, which represents the SRT values from 10 min, 5 min and 1 min (from left to right) assimilation interval experiments, respectively.

Table 1. Standard deviations of observation error ( $\sigma_o$ ) and background error ( $\sigma_b$ )

	$\sigma_o$	$\sigma_b$
$V_h$	1 m s <sup>-1</sup>	3 m s <sup>-1</sup>
w	0.667 m s <sup>-1</sup>	2 m s <sup>-1</sup>
$\theta$	0.667 K	2 K
$q_v$	0.25 g kg <sup>-1</sup>	0.75 g kg <sup>-1</sup>
$q_r$	0.1 g kg <sup>-1</sup>	0.3 g kg <sup>-1</sup>

Table 2. The list of experiments assimilating measurements, their corresponding SRT (minutes), ASED and RMSZ (dBZ) at the end of 90 minutes data assimilation.

Obs.	<i>Every minute</i>			<b>Every 5 minutes</b>			<i>Every 10 minutes</i>		
	<i>SRT</i>	<i>ASED</i>	<i>RMSZ</i>	<b>SRT</b>	<b>ASED</b>	<b>RMSZ</b>	<i>SRT</i>	<i>ASED</i>	<i>RMSZ</i>
<b>Vh</b>	32	0.001	0.3	<b>70</b>	<b>0.067</b>	<b>4.1</b>		0.210	6.7
<b>W</b>	84	0.141	4.7		<b>0.706</b>	<b>12.6</b>		0.934	20.1
<b>Pt</b>		1.963	11.4		<b>0.847</b>	<b>12.6</b>		0.896	17.6
<b>Qv</b>		0.180	6.94		<b>0.371</b>	<b>7.3</b>		0.587	9.4
<b>Qr</b>		1.402	5.1		<b>1.268</b>	<b>11.4</b>		0.891	14.3
<b>VhW</b>	29	0.002	0.4	<b>36</b>	<b>0.004</b>	<b>0.9</b>	71	0.076	3.6
<b>VhPt</b>	30	0.038	1.7	<b>28</b>	<b>0.042</b>	<b>2.1</b>	43	0.057	5.2
<b>VhQv</b>	19	0.018	2.0	<b>18</b>	<b>0.008</b>	<b>1.5</b>	25	0.020	2.0
<b>VhQr</b>	29	0.004	2.7	<b>46</b>	<b>0.025</b>	<b>2.1</b>	81	0.101	3.6
<b>VhWPt</b>	27	0.018	0.7	<b>24</b>	<b>0.030</b>	<b>1.2</b>	31	0.105	2.8
<b>VhWQv</b>	18	0.028	2.8	<b>20</b>	<b>0.006</b>	<b>1.3</b>	21	0.008	1.4
<b>VhWQr</b>	25	0.008	2.7	<b>27</b>	<b>0.007</b>	<b>1.5</b>	51	0.037	2.5

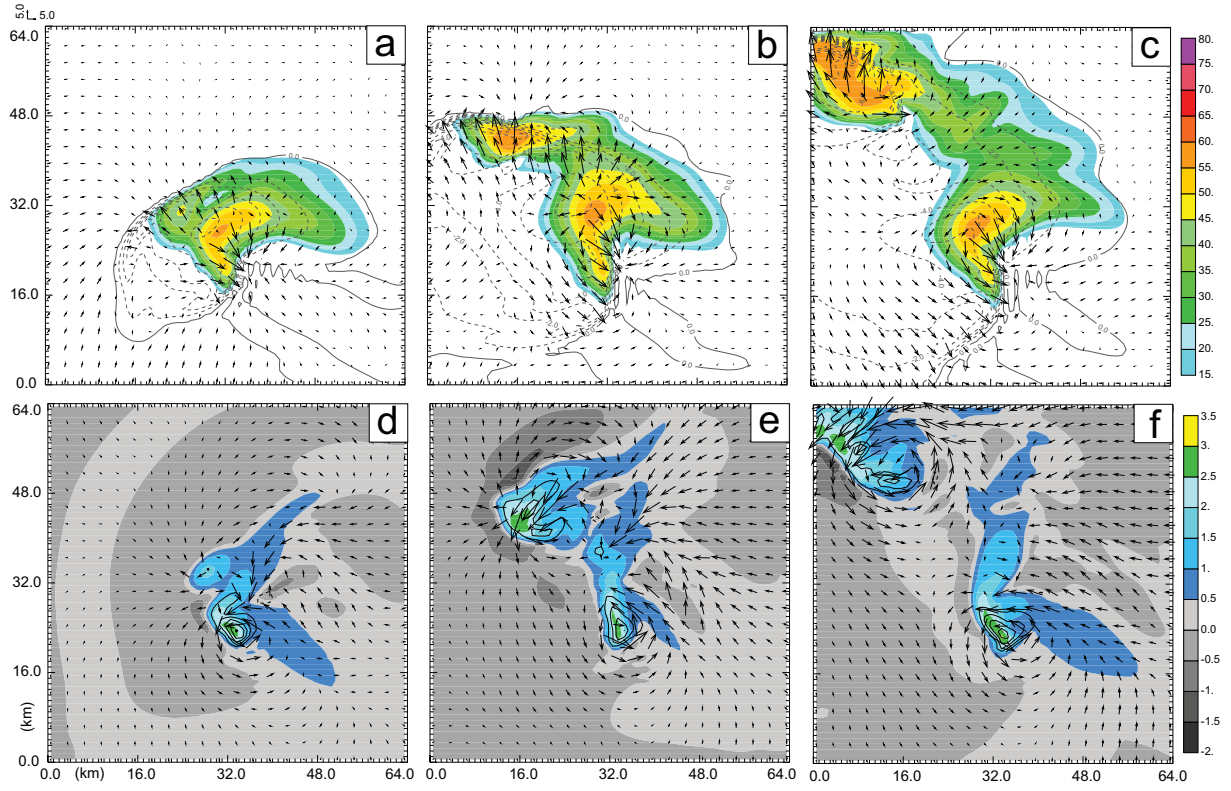


Fig. 1. (a), (b) and (c):  $\vec{V}'_h$  (vectors),  $\theta'$  (contours every 1 K) and reflectivity (shaded) at  $z = 250$  m AGL; (d), (e) and (f):  $\vec{V}'_h$  (vectors),  $w$  (contours every  $6 \text{ m s}^{-1}$ ) and  $q'_v$  (shaded) at  $z = 5$  km AGL from the simulation run every 30 minutes from 50 to 110 minutes into the truth simulation. (a) and (d)  $t = 50$  min, (b) and (e)  $t = 80$  min, (c) and (f)  $t = 110$  min.

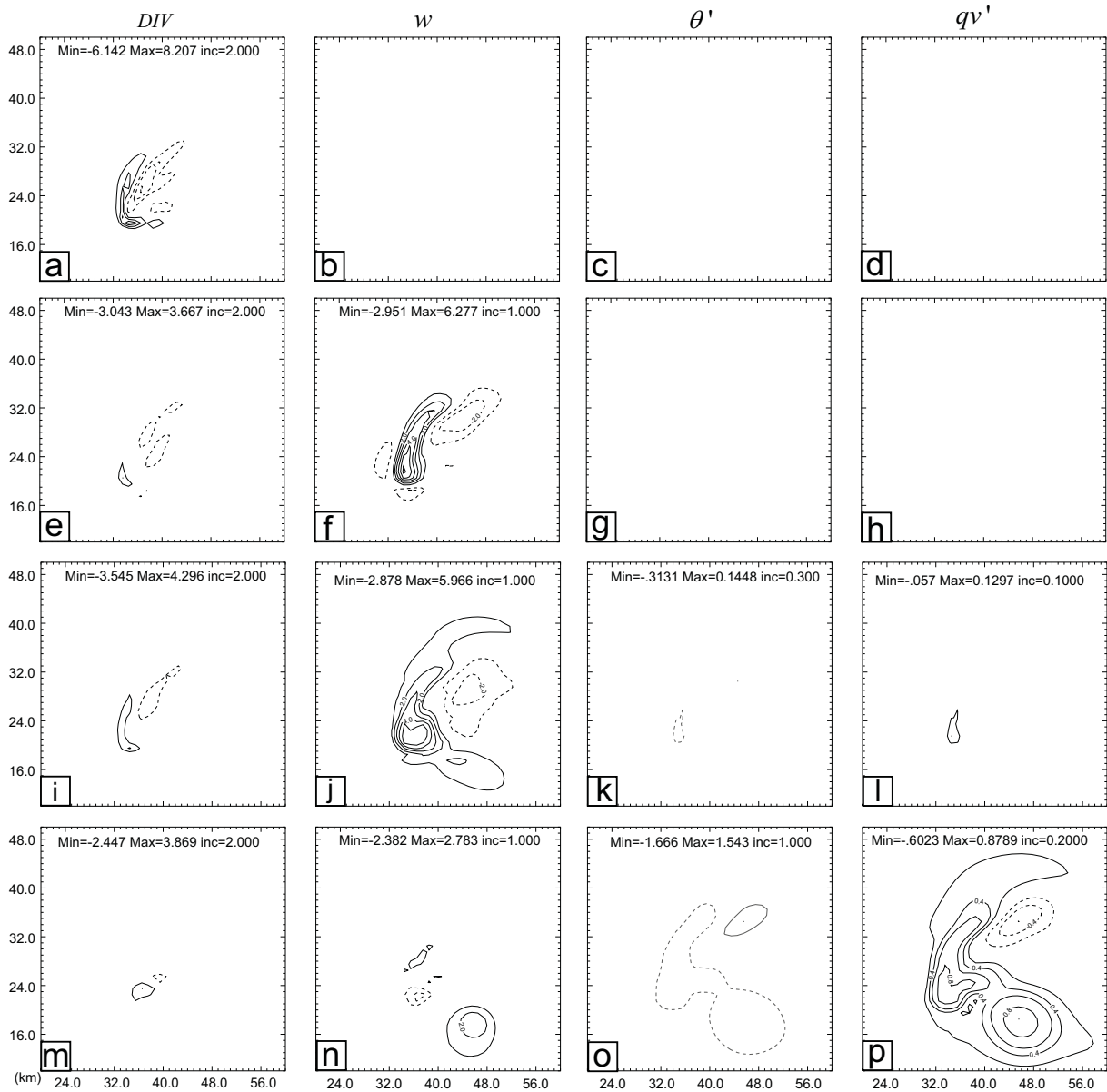


Fig. 2. The horizontal wind divergence field, vertical velocity, perturbation potential temperature, perturbation water vapor mixing ratio for experiment Vh\_5 at  $z = 4$  km AGL. (a),(b),(c),(d) are at  $t = 0$  s into the assimilation run; (e), (f), (g), (h) are at  $t = 6$  s into the assimilation run, (i),(j),(k),(l) are at  $t = 12$  s into the assimilation run; (m),(n),(o),(p) are at  $t = 300$  s into the assimilation run. (k) and (l) use different contour intervals to (o) and (p). The horizontal axis starts from 20 km and the vertical axis starts from 10 km.

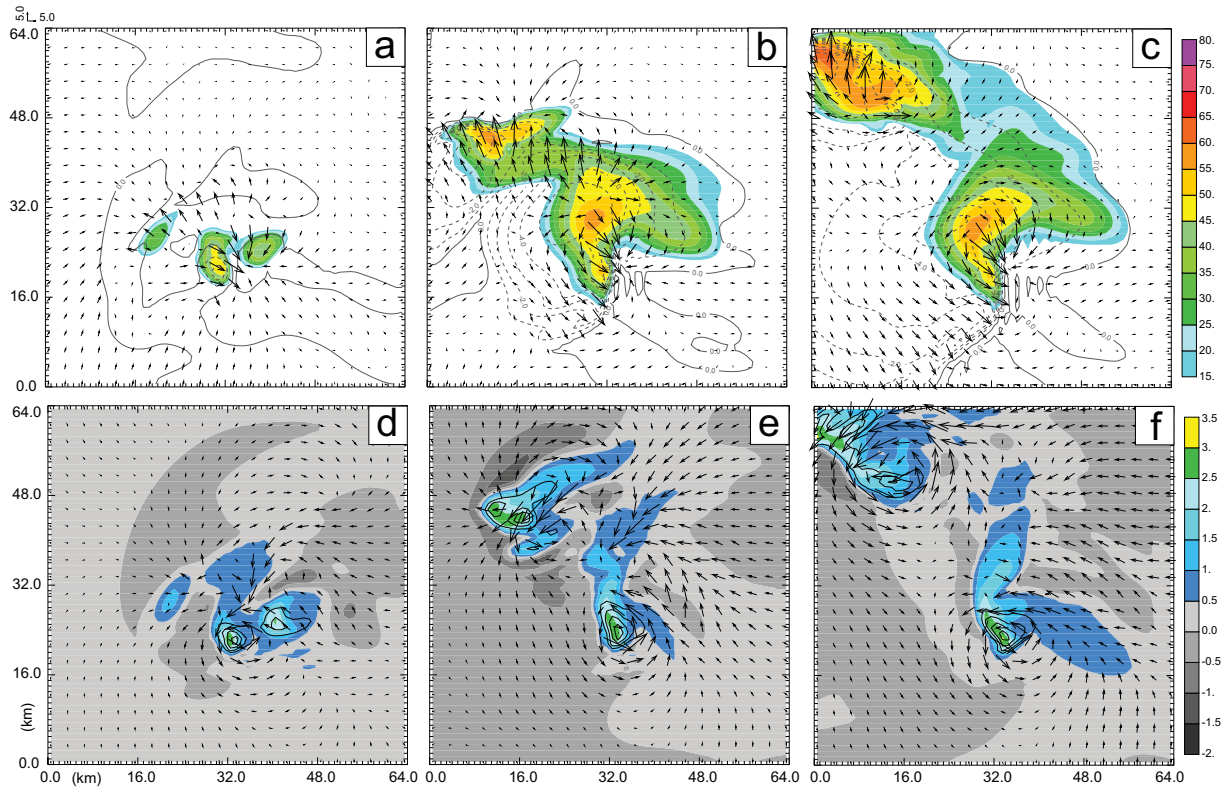


Fig. 3. (a), (b) and (c):  $\vec{V}_h'$  (vectors),  $\theta'$  (contours every 1 K) and reflectivity (shaded) at  $z = 250$  m AGL; (d), (e) and (f):  $\vec{V}_h'$  (vectors),  $w$  (contours every  $6 \text{ m s}^{-1}$ ) and  $q_v'$  (shaded) at  $z = 5$  km AGL for experiment Vh\_5 experiment every 30 minutes from 20 to 80 minutes into the assimilation run (corresponding to 50 to 110 minutes into truth simulation). (a) and (d)  $t = 20$  min, (b) and (e)  $t = 50$  min, (c) and (f)  $t = 80$  min.

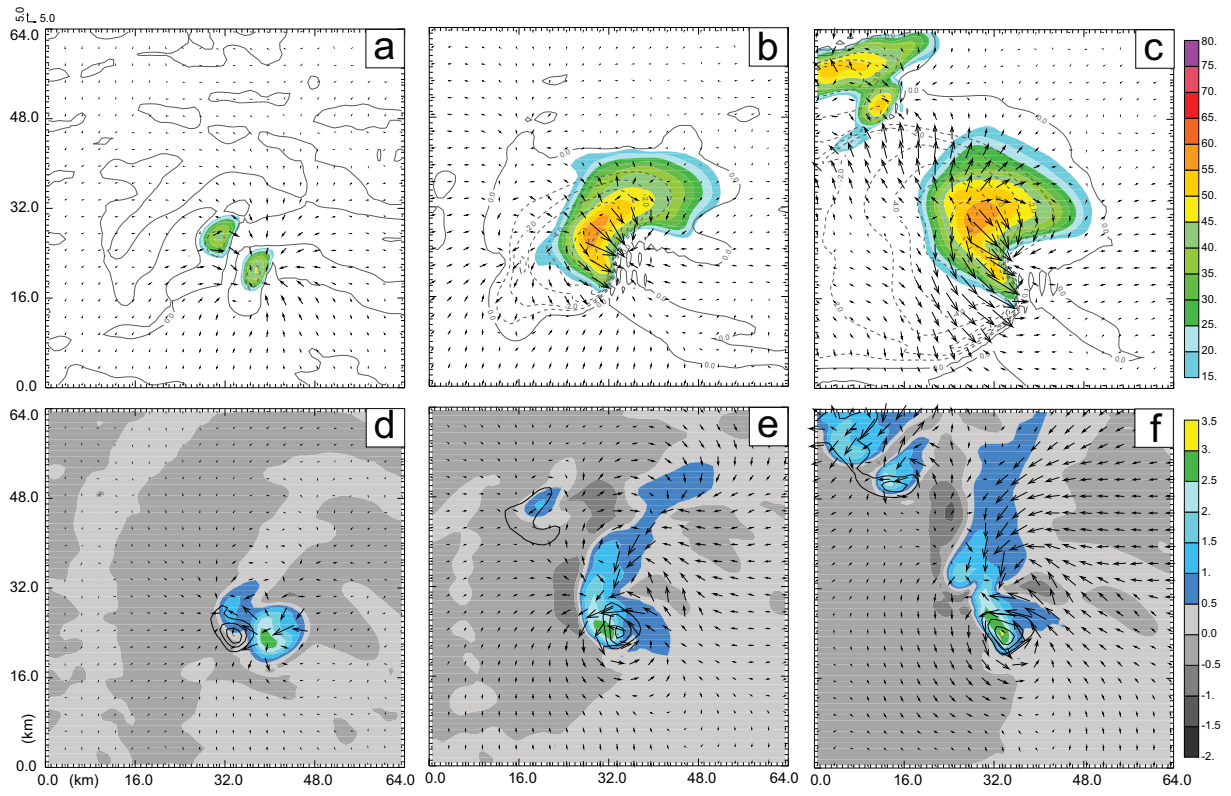


Fig. 4. Similar to Fig. 3, but for experiment W\_5 .

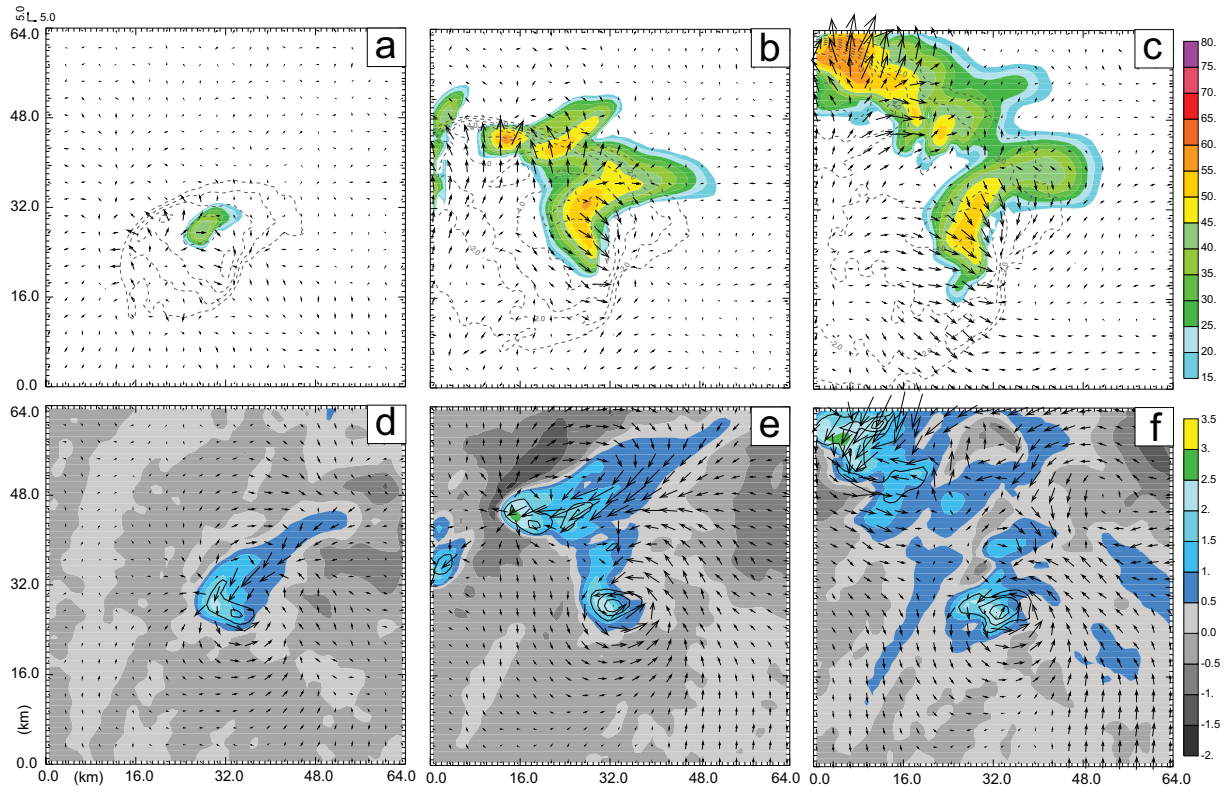


Fig. 5. Similar to Fig. 3, but for the experiment Pt\_5.

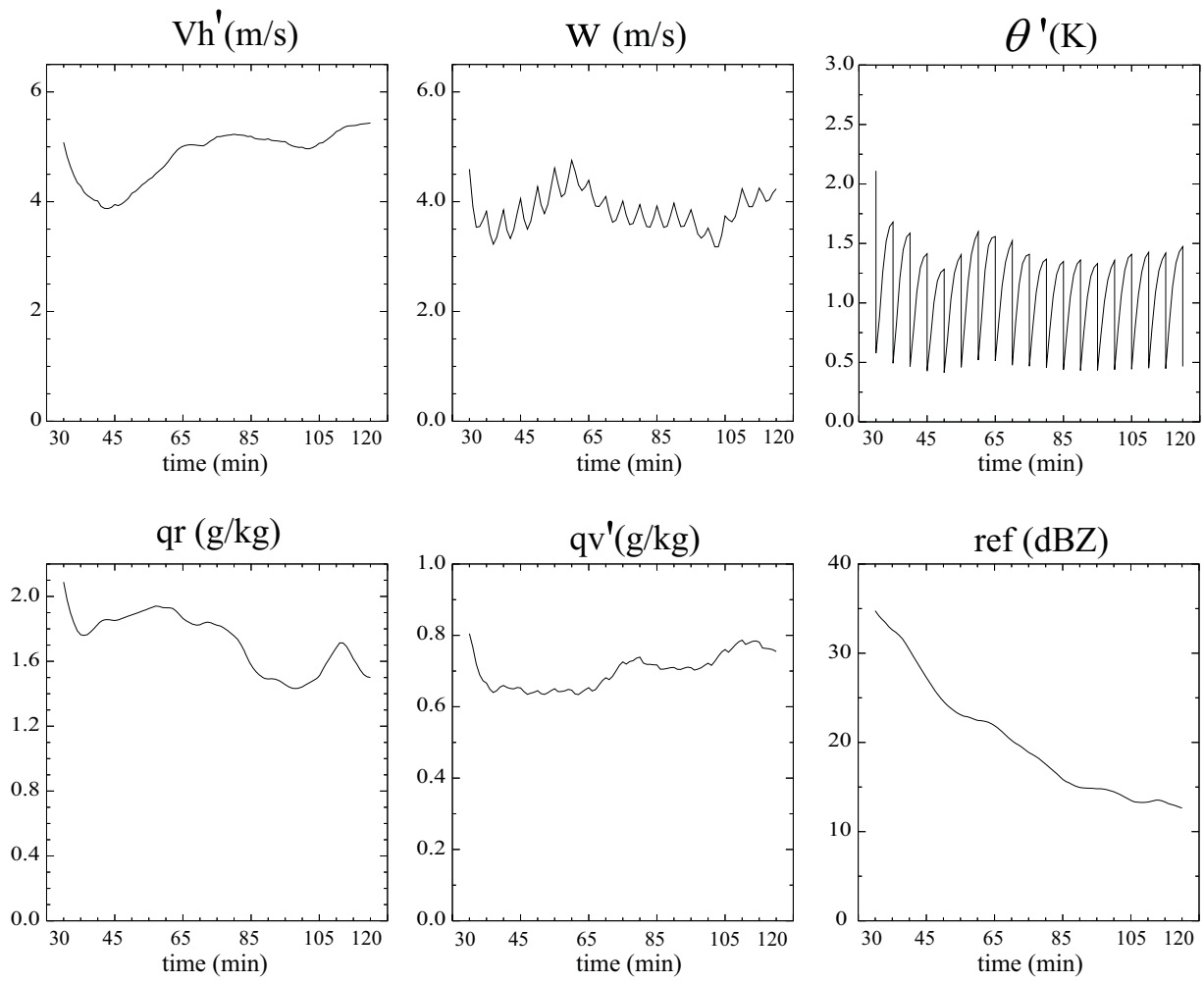


Fig. 6. The RMS errors of analyses (at 5 minute intervals) and of forecasts every minute for experiment Pt\_5. The horizontal axis shows the minutes into the truth run.

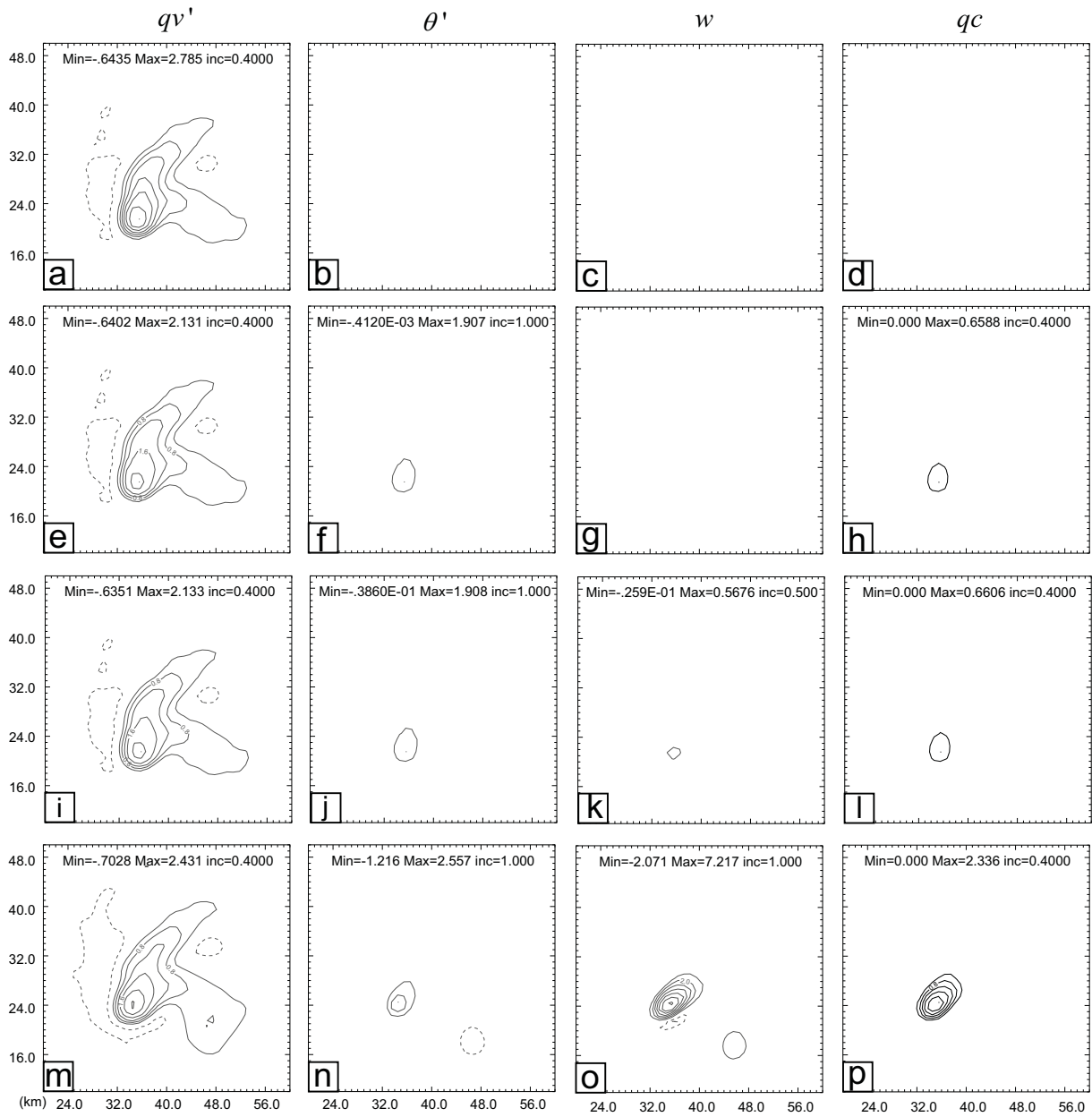


Fig. 7. The perturbation water vapor mixing ratio, perturbation potential temperature, vertical velocity, cloud water mixing ratio for experiment Qv\_5 at z = 4 km AGL. (a),(b),(c),(d) are at t = 0 s into the assimilation run; (e),(f),(g),(h) are at t = 6 s into the assimilation run, (i),(j),(k),(l) are at t = 12 s into the assimilation run; (m),(n),(o),(p) are at t = 300 s into the assimilation run. The horizontal axis starts from 20 km and the vertical axis starts from 10 km.

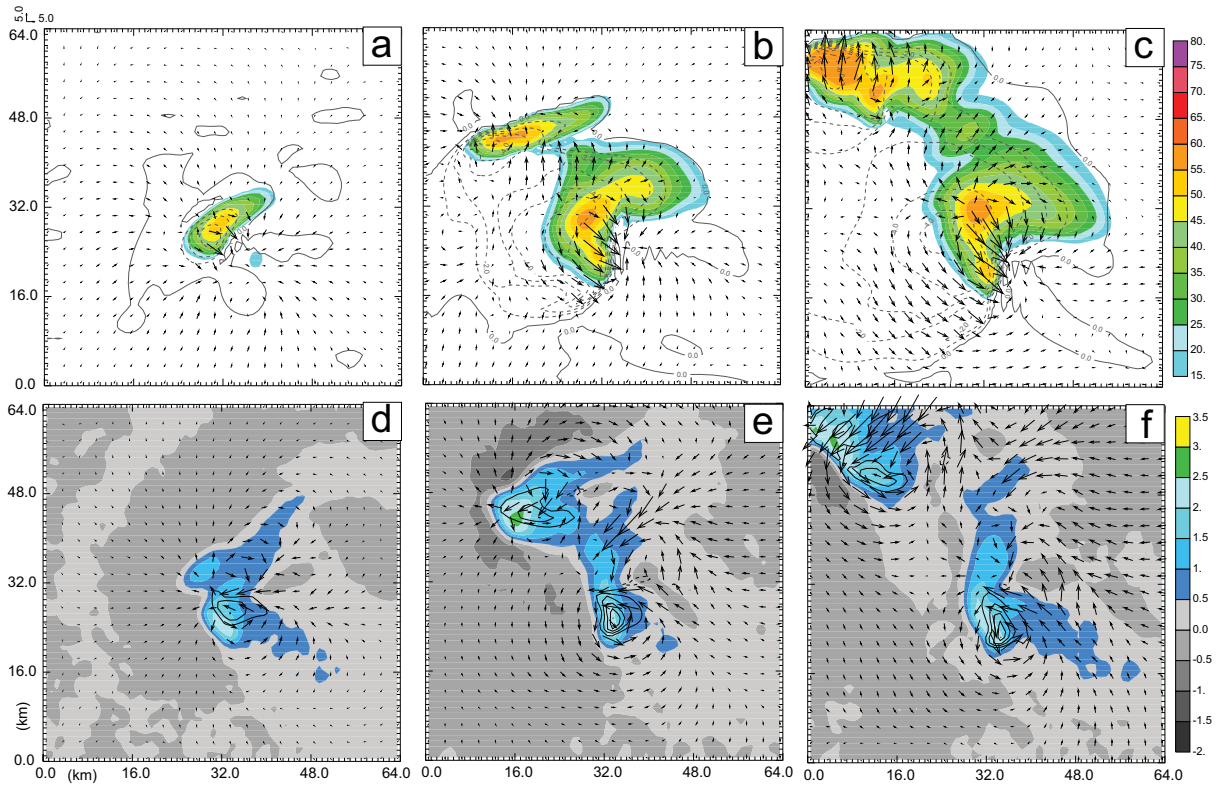


Fig. 8. Similar to Fig. 3, but for experiment Qv\_5.

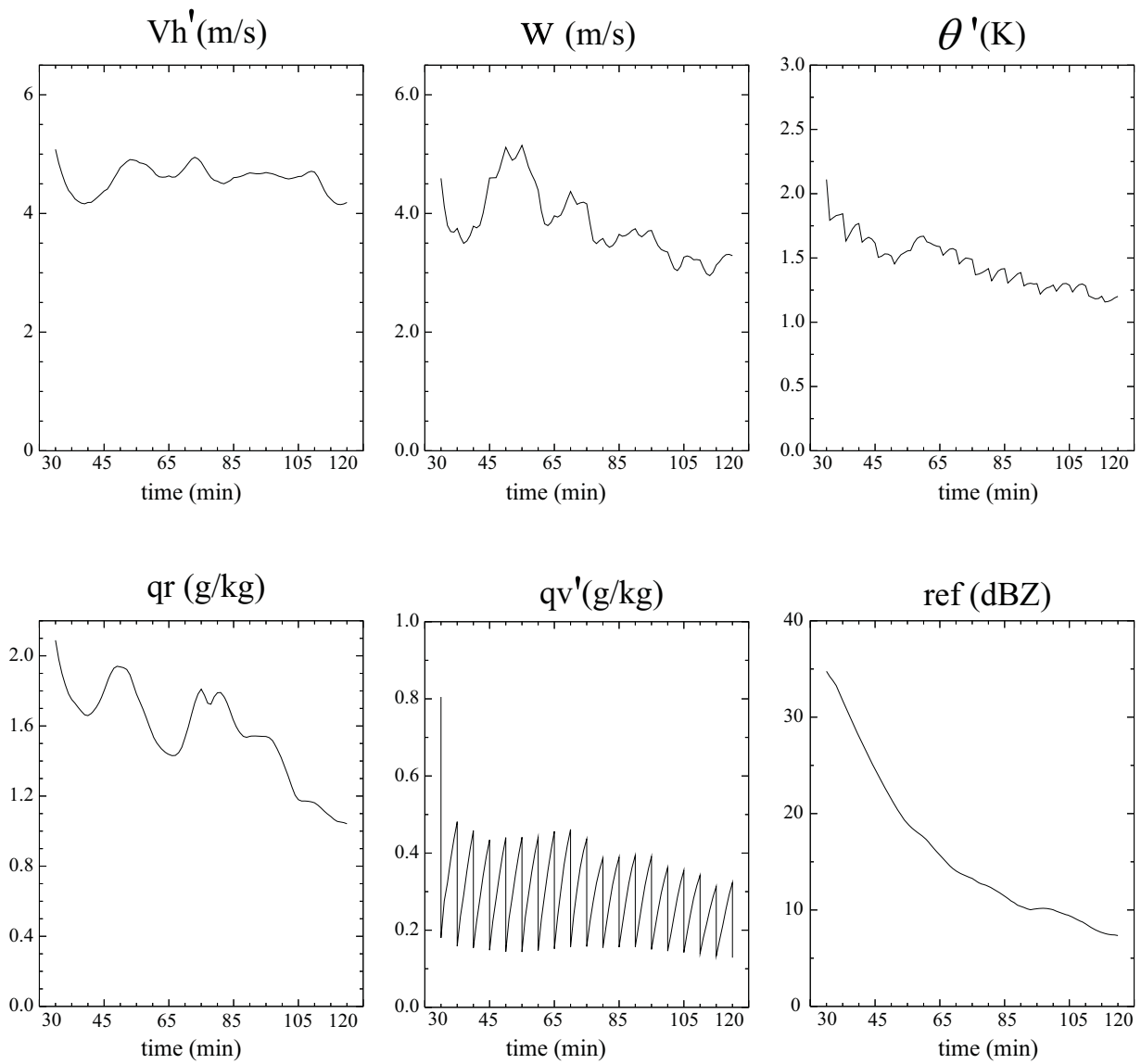


Fig. 9. The RMS errors of analyses (at 5 minute intervals) and of forecasts every minute for experiment Qv\_5. The horizontal axis shows the minutes into the truth run.

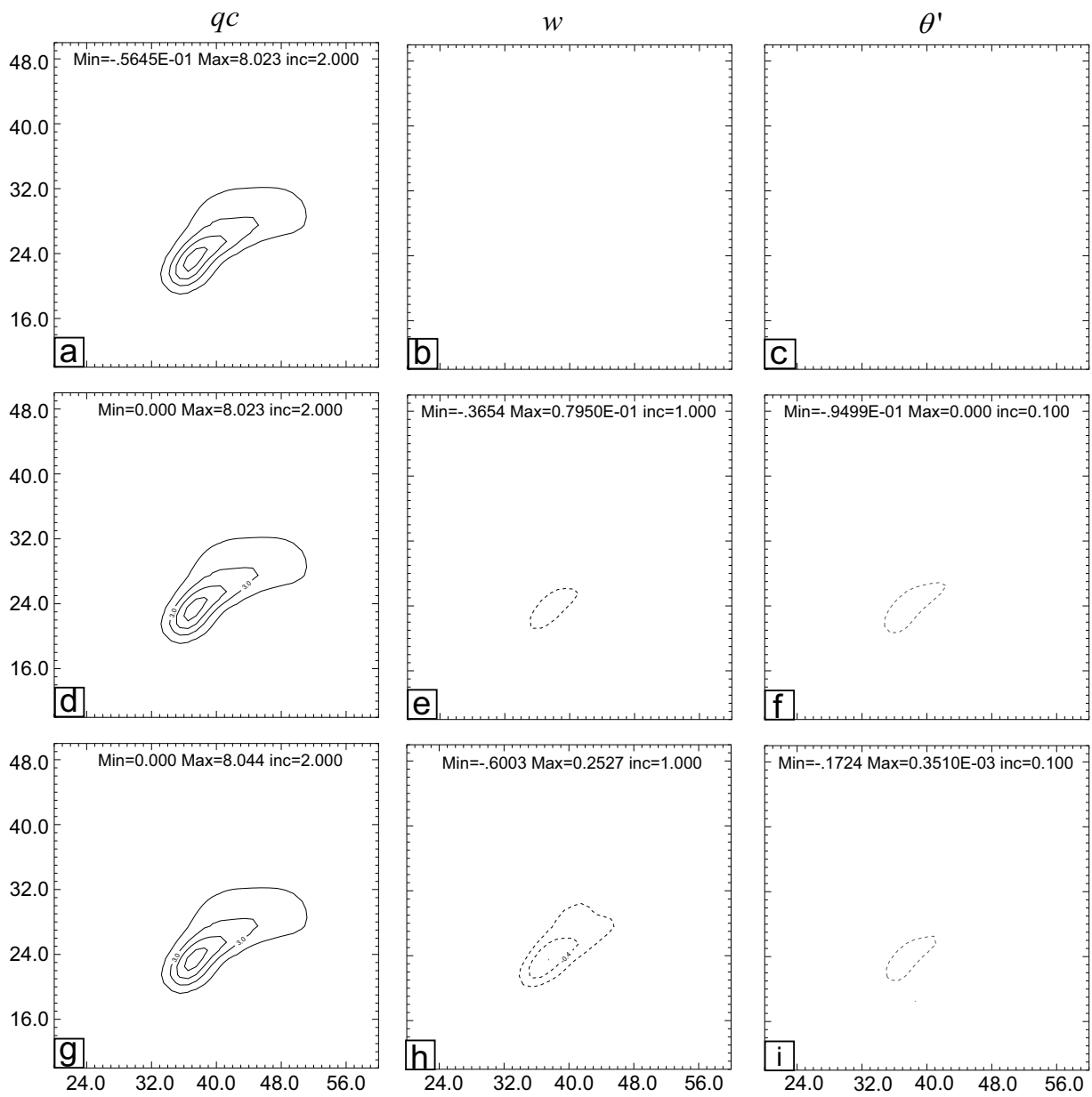


Fig. 10. The rainwater mixing ratio, vertical velocity, perturbation potential temperature from experiment Qr\_5, at  $z = 4$  km AGL. (a),(b),(c) are at  $t = 0$  s into the assimilation run; (d),(e),(f) are at  $t = 6$  s into the assimilation run, (g),(h),(i) are at  $t = 12$  s into the assimilation run. The horizontal axis starts from 20 km and the vertical axis starts from 10 km.

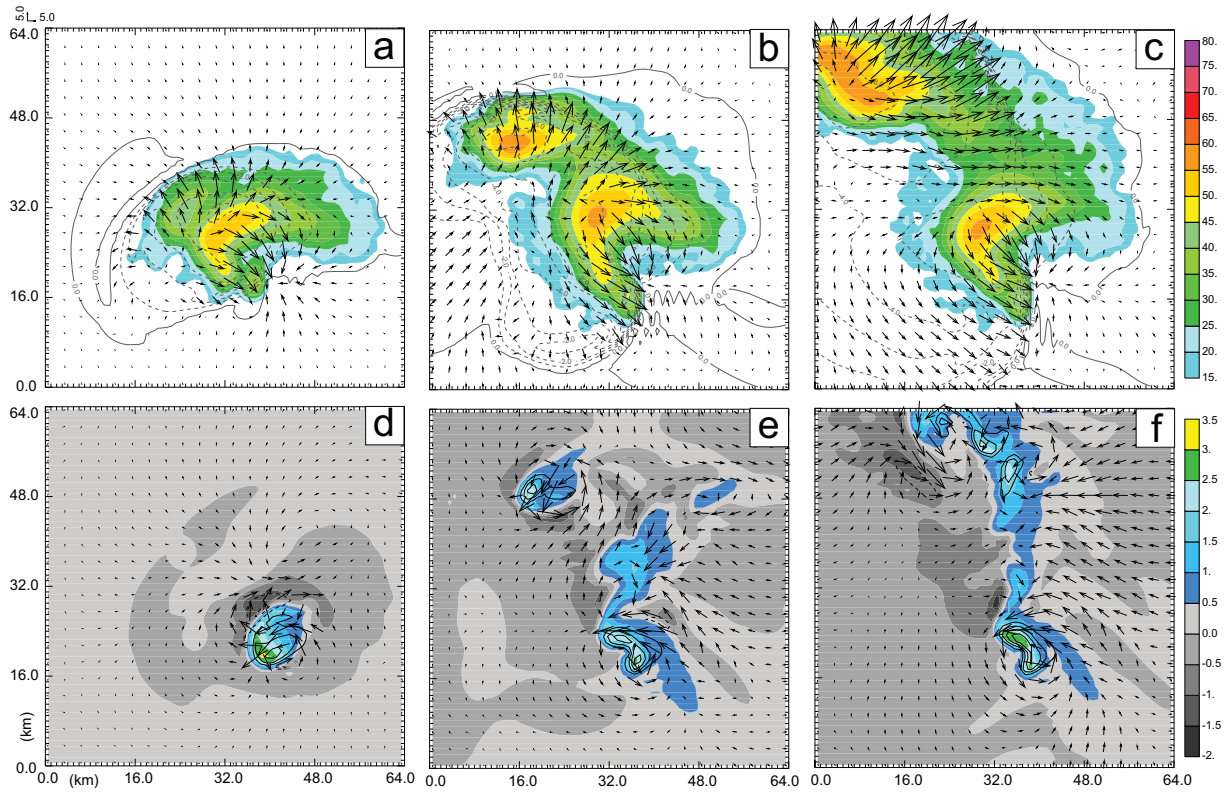


Fig. 11. Similar to Fig. 3, but for experiment Qr\_5.

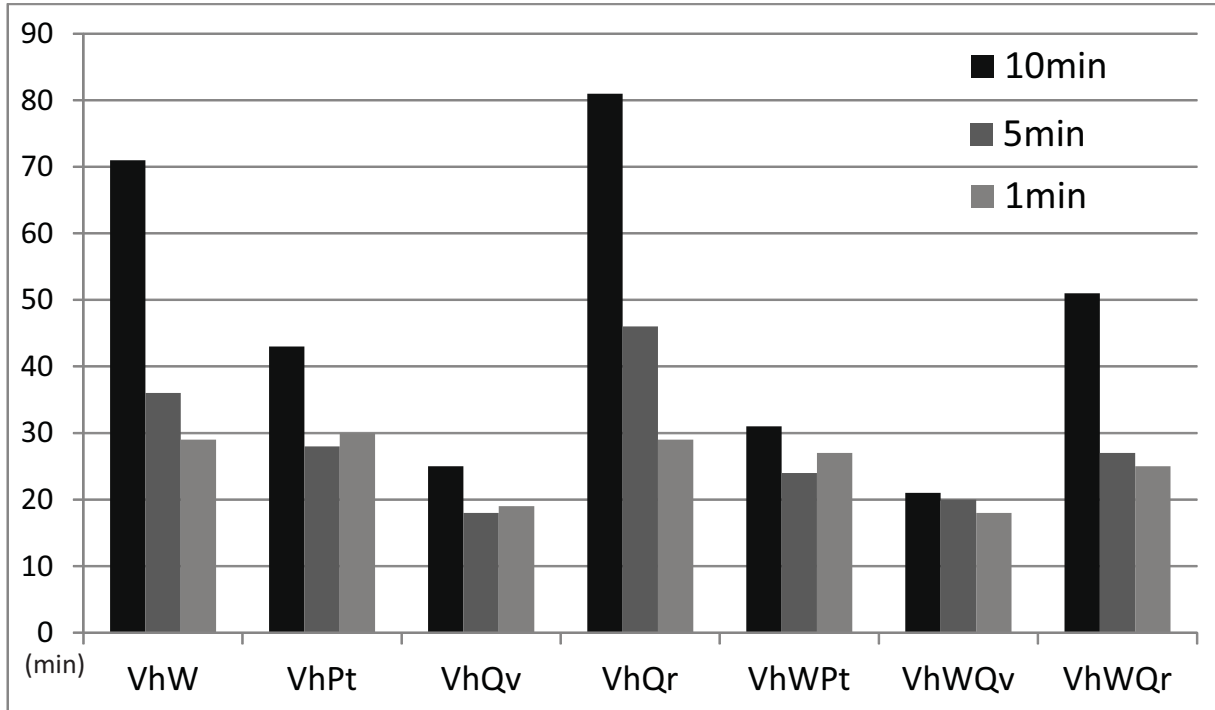


Fig. 12. Bar chart of the SRT values from experiments assimilating two- and three-types of measurements. The vertical axis shows the SRT values in unit of minutes; the horizontal axis shows different observation combinations. For each observation combination, three bars are plotted, which represents the SRT values from 10 min, 5 min and 1 min (from left to right) assimilation interval experiments, respectively.